Inorganic Chemistry
Article

Inorg. Chem. **2011**, *50*, 1551–1562 **1551**
DOI: 10.1021/ic1021627

Iron-Mediated Hydrazine Reduction and the Formation of Iron-Arylimide Heterocubanes

Michael J. Zdilla,[†] Atul K. Verma,[‡] and Sonny C. Lee*

Department of Chemistry, Princeton University, Princeton, New Jersey 08544, United States and Department of Chemistry, University of Waterloo, Waterloo, Ontario, Canada N2L 3G1.
[†]Current address: Department of Chemistry, Temple University, Philadelphia, Pennsylvania 19122.
[‡]Current address: Avecia Biotechnology, Inc., Milford, Massachusetts 01757

Received October 27, 2010

The reaction of $Fe(N\{SiMe_3\}_2)_2$ (**1**) with 1 equiv of arylthiol (ArSH) results in material of notional composition $Fe(SAr)(N\{SiMe_3\}_2)$ (**2**), from which crystalline $Fe_2(\mu\text{-}SAr)_2(N\{SiMe_3\}_2)_2(THF)_2$ (Ar = Mes) can be isolated from tetrahydrofuran (THF) solvent. Treatment of **2** with 0.5 equiv of 1,2-diarylhydrazine (Ar′NH−NHAr′, Ar′ = Ph, *p*-Tol) yields ferric-imide-thiolate cubanes $Fe_4(\mu_3\text{-}NAr')_4(SAr)_4$ (**3**). The site-differentiated, 1-electron reduced iron-imide cubane derivative $[Fe(THF)_6][Fe_4(\mu_3\text{-}N\text{-}p\text{-}Tol)_4(SDMP)_3(N\{SiMe_3\}_2)]_2$ ($[Fe(THF)_6][\mathbf{4}]_2$; DMP = 2,6-dimethylphenyl) can be isolated by adjusting the reaction stoichiometry of **1**/ArSH/Ar′NHNHAr′ to 9:6:5. The isolated compounds were characterized by a combination of structural (X-ray diffraction), spectroscopic (NMR, UV−vis, Mössbauer, EPR), and magnetochemical methods. Reactions with a range of hydrazines reveal complex chemical behavior that includes not only N−N bond reduction for 1,2-di- and trisubstituted arylhydrazines, but also catalytic disproportionation for 1,2-diarylhydrazines, N−C bond cleavage for 1,2-diisopropylhydrazine, and no reaction for hindered and tetrasubstituted hydrazines.

Introduction

The study of metal-mediated hydrazine reduction has long been associated with efforts to establish the as-yet unknown reaction chemistry of biological nitrogen fixation. The biological reduction of dinitrogen to ammonia occurs at distinctive iron−sulfur (Fe−S) biometalloclusters within nitrogenase enzymes, of which the best characterized is the iron−molybdenum cofactor (FeMo-cofactor) of molybdenum-dependent nitrogenase.[1] The transformation is reasonably assumed to proceed through some type of metal-bound hydrazinic fragment,[2] and parent hydrazine (N_2H_4) is released upon acid or base-quenching of active, presteady-state enzyme;[3] N_2H_4 is also detected as a very minor side product in vanadium-dependent nitrogenase.[4] Parent hydrazine itself can serve as a substrate for nitrogenase, although the reduction efficiency is poor in wild-type enzyme[5,6a,6c] and the relationship of this chemistry to the actual dinitrogen reduction pathway is unclear. Recently, the first spectroscopic detection of hydrazine interaction with the FeMo-cofactor has been achieved in a mutant nitrogenase.[6]

Synthetic investigations of metal-mediated hydrazine reduction are broad-ranging and span a number of transition elements and a range of different ligand environments. With respect to the metals present in the catalytic clusters of nitrogenases, the most extensive studies have focused on hydrazine reactivity in molybdenum complexes. The biological connection stems from the presence of molybdenum in the FeMo-cofactor, currently formulated with a $[MoFe_7S_9X]$ cluster core (X = C, N, or O), and it is predicated on the supposition that molybdenum, as the unique heterometal in an Fe−S environment, is the local substrate binding site within the cluster.[2]

A diversity of molybdenum systems have been explored in the context of hydrazine reduction, including mid-[7,8] to high-valent[9] mononuclear complexes, dinuclear species,[10] and heterometallic, sulfide-containing clusters,[11−13] and stoichiometric, disproportionative, and catalytic hydrazine reductions have been demonstrated. Metal-bound hydrazide

*To whom correspondence should be addressed. E-mail: sclee@uwaterloo.ca.

(1) (a) Christiansen, J.; Dean, D. R.; Seefeldt, L. C. *Annu. Rev. Plant Physiol. Plant Mol. Biol.* **2001**, *52*, 269. (b) Burgess, B. K.; Lowe, D. L. *Chem. Rev.* **1996**, *96*, 2983. (c) Eady, R. R. *Chem. Rev.* **1996**, *96*, 3013.

(2) Seefeldt, L. C.; Hoffman, B. M.; Dean, D. R. *Annu. Rev. Biochem.* **2009**, *78*, 701.

(3) Thorneley, R. N. F.; Lowe, D. J. In *Molybdenum Enzymes*; Spiro, T. G., Ed.; Wiley-Interscience: New York, 1985; p 221.

(4) (a) Dilworth, M. J.; Eldridge, M. E.; Eady, R. R. *Biochem. J.* **1993**, *289*, 395. (b) Dilworth, M. J.; Eady, R. R. *Biochem. J.* **1991**, *277*, 465.

(5) Davis, L. C. *Arch. Biochem. Biophys.* **1980**, *204*, 270.

(6) (a) Barney, B. M.; Laryukhin, M.; Igarashi, R. Y.; Lee, H.-I.; Dos Santos, P. C.; Yang, T.-C.; Hoffman, B. M.; Dean, D. R.; Seefeldt, L. C. *Biochemistry* **2005**, *44*, 8030. (b) Barney, B. M.; Yang, T.-C.; Igarashi, R. Y.; Dos Santos, P. C.; Laryukhin, M.; Lee, H.-I.; Hoffman, B. M.; Dean, D. R.; Seefeldt, L. C. *J. Am. Chem. Soc.* **2005**, *127*, 14960. (c) Barney, B. M.; Igarashi, R. Y.; Dos Santos, P. C.; Dean, D. R.; Seefeldt, L. C. *J. Biol. Chem.* **2004**, *279*, 53621.

Published on Web 01/20/2011

($M=N-NH_2$) species are proposed as key intermediates in dinitrogen reduction at mononuclear centers,[14] and appropriate species have exhibited the relevant stepwise reactivity.[7] From a bioinorganic standpoint, we note studies of the catalytic chemical reduction of parent hydrazine by Fe−S and M−Fe-S (M = Mo, V) cubane species that strongly resemble, in whole or in part, known biological clusters;[12] under the reported conditions, only labile, heterometal-substituted clusters were active in hydrazine reduction, suggesting the need for a reactive heterometal site in this chemistry.[15] With the discovery of vanadium-dependent nitrogenase,[1c] vanadium has also been investigated in the same context and with similar chemistry, although these studies are much more limited in number and scope.[16]

Recent attention on this subject has expanded to include iron-mediated chemistry. Iron-based biological nitrogen fixation appears to be required in at least one class of nitrogenase that contains no transition elements other than iron.[1c] The focus on iron intensified following the macromolecular crystallographic studies that yielded the first molecular visualization of the entire FeMo-cofactor;[17] the structural data inspired mechanistic conjectures that specifically enlisted iron centers as the site of substrate reduction chemistry in the heterometallic cofactor cluster.[18] The recent detection of nitrogenase intermediates in site-directed Mo-dependent nitrogenase mutants has also implicated iron in substrate binding based on the positions of the introduced protein side chain substitutions.[19]

In comparison with the molybdenum chemistry, examples of iron-mediated hydrazine reduction are fewer in number and generally postdate the first nitrogenase protein structure determinations. The earliest report to our knowledge is an account, without molecular details, of the catalytic electrochemical reduction of N_2H_4 by $[Fe_4S_4(SR)_4]^{2-}$ cubane clusters.[13] More recently, the reduction of parent hydrazine has been found in β-diketiminate[20] and polyphosphine[21] complexes of Fe(II) and, catalytically, in a dinuclear cyclopentadienyl/thiolate system.[22] Reductive cleavage of the N−N bond in organohydrazines and ligated organohydrazides has also been observed in the last system, as well as in a few other mono- and dinuclear complexes with cyclopentadienyl[23] and β-diketiminate[24] ancillary ligands. These examples of Fe-mediated hydrazine reduction, while few in number, nevertheless encompass a range of coordination environments and reaction conditions. Although detailed mechanistic studies are few,[24c,25] the body of evidence suggests a number of fundamentally different hydrazine reduction pathways depending on reaction system.

In our own studies, we have assembled Fe(III)-arylimide-thiolate cubane clusters, $Fe_4(NAr')_4(SAr)_4$, by reductive scission of the N−N bond in 1,2-diarylhydrazines.[26] With respect to potentially relevant biomimetic chemistry, this reaction system attracts our interest because of features in common with biological Fe−S centers: (1) the iron sites are weak-field, tetrahedral, and possess a partial sulfur-anion environment; (2) the reaction chemistry couples substrate reduction to biologically observed Fe(II)/Fe(III) redox states; and (3) the product cluster structure maps onto the archetypal biological Fe−S cubane geometry. Following an initial communication,[26] we present here a detailed account

(7) Mo(IV)-hydrazide(2−) complexes from protonated Mo(0)-dinitrogen precursors: (a) Baumann, J. A.; Bossard, G. E.; George, T. A.; Howell, D. B.; Koczon, L. M.; Lester, R. K.; Noddings, C. M. *Inorg. Chem.* **1985**, *24*, 3568. (b) Gebreyes, K.; Zubieta, J.; George, T. A.; Koczon, L. M.; Tisdale, R. C. *Inorg. Chem.* **1986**, *25*, 405. (c) Kaul, B. B.; Hayes, R. K.; George, T. A. *J. Am. Chem. Soc.* **1990**, *112*, 2002. (d) Galindo, A.; Hills, A.; Hughes, D. L.; Richards, R. L.; Hughes, M.; Mason, J. *J. Chem. Soc., Dalton Trans.* **1990**, 283. (e) George, T. A.; Rose, D. J.; Chang, Y.; Chen, Q.; Zubieta, J. *Inorg. Chem.* **1995**, *34*, 1295.

(8) (a) Hitchcock, P. B.; Hughes, D. L.; Maguire, M. J.; Marjani, K.; Richards, R. L. *J. Chem. Soc., Dalton Trans.* **1997**, 4747. (b) Watanabe, D.; Gondo, S.; Seino, H.; Mizobe, Y. *Organometallics* **2007**, *26*, 4909.

(9) (a) Schrock, R. R.; Glassman, T. E.; Vale, M. G. *J. Am. Chem. Soc.* **1991**, *113*, 725. (b) Vale, M. G.; Schrock, R. R. *Inorg. Chem.* **1993**, *32*, 2767. (c) Carrillo, D. *C. R. Acad. Sci. II C* **2000**, *3*, 175. (d) Yandulov, D. V.; Schrock, R. R. *J. Am. Chem. Soc.* **2002**, *124*, 6252. (e) Yandulov, D. V.; Schrock, R. R.; Rheingold, A. L.; Ceccarelli, C.; Davis, W. M. *Inorg. Chem.* **2003**, *42*, 796. (f) Yandulov, D. V.; Schrock, R. R. *Inorg. Chem.* **2005**, *44*, 1103. (g) Vrubel, H.; Verzenhassi, V. H. C.; Nakagaki, S.; Nunes, F. S. *Inorg. Chem. Commun.* **2008**, *11*, 1040.

(10) (a) Block, E.; Ofori-Okai, G.; Kang, H.; Zubieta, J. *J. Am. Chem. Soc.* **1992**, *114*, 758. (b) Schollhammer, P.; Petillon, F. Y.; PoderGuillou, S.; Saillard, J. Y.; Talarmin, J.; Muir, K. W. *Chem. Commun.* **1996**, 2633. (c) Schollhammer, P.; Guenin, E.; Petillon, F. Y.; Talarmin, J.; Muir, K. W.; Yufit, D. S. *Organometallics* **1998**, *17*, 1922. (d) Petillon, F. Y.; Schollhammer, P.; Talarmin, J.; Muir, K. W. *Inorg. Chem.* **1999**, *38*, 1954. (e) Le Grand, N.; Muir, K. W.; Petillon, F. Y.; Pickett, C. J.; Schollhammer, P.; Talarmin, J. *Chem.—Eur. J.* **2002**, *8*, 3115. (f) Schollhammer, P.; Didier, B.; Le Grand, N.; Petillon, F. Y.; Talarmin, J.; Muir, K. W.; Teat, S. J. *Eur. J. Inorg. Chem.* **2002**, 658.

(11) (a) Masumori, T.; Seino, H.; Mizobe, Y.; Hidai, M. *Inorg. Chem.* **2000**, *39*, 5002. (b) Seino, H.; Masumori, T.; Hidai, M.; Mizobe, Y. *Organometallics* **2003**, *22*, 3424. (c) Takei, I.; Dohki, K.; Kobayashi, K.; Suzuki, T.; Hidai, M. *Inorg. Chem.* **2005**, *44*, 3768.

(12) (a) Coucouvanis, D.; Mosier, P. E.; Demadis, K. D.; Patton, S.; Malinak, S. M.; Kim, C. G.; Tyson, M. A. *J. Am. Chem. Soc.* **1993**, *115*, 12193. (b) Demadis, K. D.; Coucouvanis, D. *Inorg. Chem.* **1994**, *33*, 4195. (c) Demadis, K. D.; Coucouvanis, D. *Inorg. Chem.* **1995**, *34*, 3658. (d) Demadis, K. D.; Malinak, S. M.; Coucouvanis, D. *Inorg. Chem.* **1996**, *35*, 4038. (e) Coucouvanis, D.; Demadis, K. D.; Malinak, S. M.; Mosier, P. E.; Tyson, M. A.; Laughlin, L. J. *J. Mol. Catal. A: Chem.* **1996**, *107*, 123.

(13) Hozumi, Y.; Imasaka, Y.; Tanaka, K.; Tanaka, T. *Chem. Lett.* **1983**, 897.

(14) (a) Pickett, C. J. *J. Biol. Inorg. Chem.* **1996**, *1*, 601. (b) Chatt, J.; Dilworth, J. R.; Richards, R. L. *Chem. Rev.* **1978**, *78*, 589. (c) Schrock, R. R. *Pure Appl. Chem.* **1997**, *69*, 2197.

(15) Coucouvanis, D. *J. Biol. Inorg. Chem.* **1996**, *1*, 594.

(16) (a) Rehder, D.; Woitha, C.; Priebsch, W.; Gailus, H. *J. Chem. Soc., Chem. Commun.* **1992**, 364. (b) Lefloch, C.; Henderson, R. A.; Hughes, D. L.; Richards, R. L. *J. Chem. Soc., Chem. Commun.* **1993**, 175. (c) Gailus, H.; Woitha, C.; Rehder, D. *J. Chem. Soc., Dalton Trans.* **1994**, 3471. (d) Malinak, S. M.; Demadis, K. D.; Coucouvanis, D. *J. Am. Chem. Soc.* **1995**, *117*, 3126. (e) Ferguson, R.; Solari, E.; Floriani, C.; Osella, D.; Ravera, M.; Re, N.; Chiesi-Villa, A.; Rizzoli, C. *J. Am. Chem. Soc.* **1997**, *119*, 10104. (f) Davies, S. C.; Hughes, D. L.; Janas, Z.; Jerzykiewicz, L. B.; Richards, R. L.; Sanders, J. R.; Silverston, J. E.; Sobota, P. *Inorg. Chem.* **2000**, *39*, 3485. (g) Davies, S. C.; Hughes, D. L.; Janas, Z.; Jerzykiewicz, L. B.; Richards, R. L.; Sanders, J. R.; Silverston, J. E.; Sobota, P. *Inorg. Chem.* **2000**, *39*, 3485. (h) Chu, W.-C.; Wu, C.-C.; Hsu, H.-F. *Inorg. Chem.* **2006**, *45*, 3164.

(17) See: Einsle, O.; Tezcan, F. A.; Andrade, S.; Schmid, B.; Yoshida, M.; Howard, J. B.; Rees, D. C. *Science* **2002**, *297*, 1696, and references therein.

(18) Peters, J. W.; Szilagyi, R. K. *Curr. Opin. Chem. Biol.* **2006**, *10*, 101.

(19) (a) Hoffman, B. M.; Dean, D. R.; Seefeldt, L. C. *Acc. Chem. Res.* **2009**, *42*, 609. (b) Dos Santos, P. C.; Igarashi, R. Y.; Lee, H.-I.; Hoffman, B. M.; Seefeldt, L. C.; Dean, D. R. *Acc. Chem. Res.* **2005**, *38*, 208.

(20) Yu, Y.; Brennessel, W. W.; Holland, P. L. *Organometallics* **2007**, *26*, 3217.

(21) (a) Crossland, J. L.; Zakharov, L. N.; Tyler, D. R. *Inorg. Chem.* **2007**, *46*, 10476. (b) Saouma, C. T.; Müller, P.; Peters, J. C. *J. Am. Chem. Soc.* **2009**, *131*, 10358.

(22) Chen, Y.; Zhou, Y.; Chen, P.; Tao, Y.; Li, Y.; Qu, J. *J. Am. Chem. Soc.* **2008**, *130*, 15250.

(23) Ohki, Y.; Takikawa, Y.; Hatanaka, T.; Tatsumi, K. *Organometallics.* **2006**, *25*, 3111.

(24) (a) Smith, J. M.; Lachicotte, R. J.; Holland, P. L. *J. Am. Chem. Soc.* **2003**, *125*, 15752. (b) Vela, J.; Stoian, S.; Flaschenriem, C. J.; Münck, E.; Holland, P. L. *J. Am. Chem. Soc.* **2004**, *126*, 4522. (c) Sadique, A. R.; Gregory, E. A.; Brennessel, W. W.; Holland, P. L. *J. Am. Chem. Soc.* **2007**, *129*, 8112.

(25) Yelle, R. B.; Crossland, J. L.; Szymczak, N. K.; Tyler, D. R. *Inorg. Chem.* **2009**, *48*, 861.

(26) Verma, A. K.; Lee, S. C. *J. Am. Chem. Soc.* **1999**, *121*, 10838.

Scheme 1

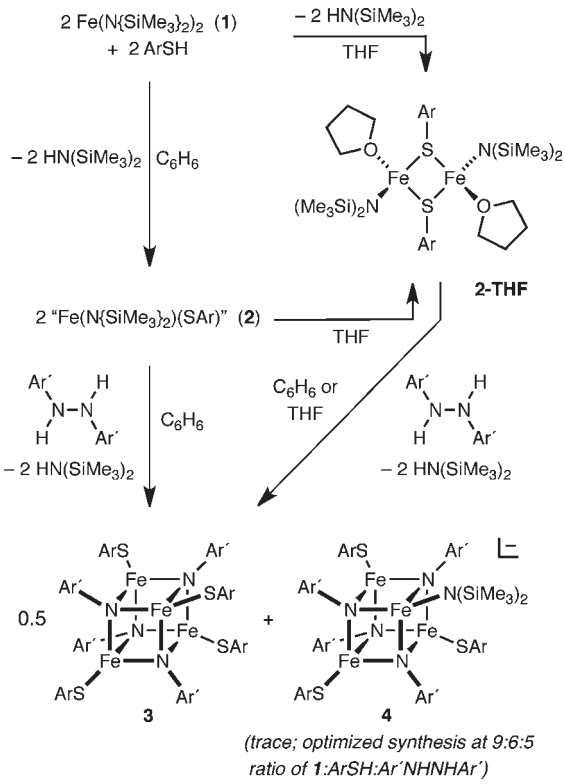

of this synthetic chemistry as well as an investigation of the scope of the hydrazine reduction.

Results and Discussion

Syntheses. The cluster synthesis chemistry is summarized in Scheme 1.

(a) Ferrous Amide Thiolate Precursor. The starting point for our syntheses is the ferrous amide precursor $Fe(N\{SiMe_3\}_2)_2$ (**1**).[27] The bis(trimethylsilyl)amide ligation in **1** provides both a strong latent base and a steric barrier for selective protolysis chemistry, allowing the introduction of a partial thiolate environment by treatment with 1 equiv of arylthiol (ArSH). With very hindered chalcogenols (e.g., 2,6-diphenylbenzenethiol), $Fe_2(\mu\text{-}QR)_2(N\{SiMe_3\}_2)_2$ (Q = O, S, Se) dimers with three-coordinate iron centers are the known products of this reaction.[28]

In our investigation, the less hindered mesitylthiol (MesSH) was employed. Protolysis gives an immediate solution color change from transparent blue (in tetrahydrofuran (THF)) or green (benzene) to dark red-brown. Reactions in benzene did not yield well-defined material (**2**, vide infra), whereas in THF reaction medium, crystalline yellow $Fe_2(SMes)_2(N\{SiMe_3\}_2)_2(THF)_2$ (**2-THF**) is readily isolated in about 50% yield. Complex **2-THF** represents a solvent adduct of the three-coordinate iron dimers obtained with very hindered chalcogenolates. We have also explored the use of other arylthiols (Ar = 2,6-dimethylphenyl, 2,4,6-diisopropylphenyl, 2-methylphenyl, phenyl) in this chemistry. Although we have not pursued their isolation at the heteroleptic ferrous amide/thiolate stage, it seems likely that these other aryl substituents exhibit similar chemistry based on equivalent reactions between *p*-tolylthiol and 2,4,6-triisopropylbenzeneselenol and **1** and $Mn(N\{SiMe_3\}_2)_2$, respectively, which yield structural congeners of **2-THF**.[29,30]

Dinuclear **2-THF** exhibits a complex ^{1}H NMR spectrum in C_6D_6 with a greater-than-expected number of signals that suggest speciation. A characteristic, simplified spectrum can be obtained in THF-d_8 solvent that is identical for both pure **2-THF** and for the protolysis product **2** obtained from reaction in benzene solvent. On the basis of this observation, we consider the product **2** from 1:1 MesSH/**1** protolysis in benzene (the typical initial in situ precursor state for the hydrazine reduction/cluster assembly chemistry that follows) as a reactive material of empirical formulation $Fe(SAr)(N\{SiMe_3\}_2)$. We attribute the isolation difficulties in the benzene reaction system to the speciation behavior observed in C_6D_6, which likely reflects oligomerization equilibria that are suppressed in the presence of coordinating THF solvent.

(b) Hydrazine Reduction and Cubane Formation. The reaction of either **2-THF** (1 equiv) or **2** (2 equiv, assuming the notional $Fe(SAr)(N\{SiMe_3\}_2)$ composition) with 1 equiv of 1,2-diarylhydrazine ($Ar'NH-NHAr'$) results in an immediate darkening of solution color from red-brown to maroon-black. After filtration to remove black, benzene-insoluble material, concentration and addition of a precipitating solvent yields the neutral cubane cluster type $Fe_4(NAr')_4(SAr)_4$ (**3**) in black microcrystalline form. Similar results are obtained using either benzene or THF as the reaction solvent. Several variations of **3** have been shown to form by ^{1}H NMR spectroscopy (Ar = Mes, 2,6-dimethylphenyl (DMP), 2,4,6-triisopropylphenyl, 2,4,6-triphenylphenyl; Ar′ = Ph, *p*-Tol).[26] The presence of 2,6-substituents on the thiolate aryl group appears to be required for the formation of stable cluster products; reactivity is observed with Ar = Ph or 2-methylphenyl, as evidenced by solution color changes to black, but no signals associated with paramagnetic species were observed by NMR spectroscopy. We speculate that less-hindered arylthiolates favor oligomerization and/or speciation to ill-defined products. We focus in this report on mesitylthiolate-ligated clusters with Ar′ = Ph (**3a**) and *p*-Tol (**3b**).

The experimental stoichiometry fits the hypothetical balanced cluster assembly reaction described by eq 1. Clusters **3a** and **3b** are isolated in about 50% yield, with azoarenes present as side products at significant levels. The possible implications of azoarene formation in relation to eq 1, hydrazine reduction, and cluster assembly mechanism are considered in a subsequent section.

$$4Fe(N\{SiMe_3\}_2)_2 + 4ArSH + 2Ar'NHNHAr' \rightarrow Fe_4(NAr')_4(SAr)_4 + 8HN(SiMe_3)_2 \quad (1)$$

(27) (a) Andersen, R. A.; Faegri, K.; Green, J. C.; Haaland, A.; Lappert, M. F.; Leung, W. P.; Rypdal, K. *Inorg. Chem.* **1988**, *27*, 1782. (b) Olmstead, M. M.; Power, P. P.; Shoner, S. C. *Inorg. Chem.* **1991**, *30*, 2547.

(28) (a) Bartlett, R. A.; Ellison, J. J.; Power, P. P.; Shoner, S. C. *Inorg. Chem.* **1991**, *30*, 2888. (b) Hauptmann, R.; Kliss, R.; Schneider, J.; Henkel, G. *Z. Anorg. Allg. Chem.* **1998**, *624*, 1927. (c) Hauptmann, R.; Kliss, R.; Henkel, G. *Angew. Chem., Int. Ed.* **1999**, *38*, 377. (d) Komuro, T.; Kawaguchi, H.; Tatsumi, K. *Inorg. Chem.* **2002**, *41*, 5083. (e) Ohta, S.; Ohki, Y.; Ikagawa, Y.; Suizu, R.; Tatsumi, K. *J. Organomet. Chem.* **2007**, *692*, 4792.

(29) Pryadun, R.; Holm, R. H. *Inorg. Chem.* **2008**, *47*, 3366.

(30) Bochmann, M.; Powell, A. K.; Song, X. *Inorg. Chem.* **1994**, *33*, 400.

A second paramagnetic cluster type is evident as a minor (< 5%) but discernible component in the ^{1}H NMR spectra of crude reaction systems. The number and relative intensities of the signals for this minority species suggested a terminally heteroleptic, C_{3v}-symmetric $[Fe_4(NAr')_4(SAr)_3(N\{SiMe_3\}_2)]^z$ cubane cluster. Reaction stoichiometries and substituents (Ar = Mes, DMP; Ar′ = Ph, *p*-Tol) were adjusted to optimize the formation and isolation of this new cluster, resulting ultimately in confirmation of the cluster identity as the salt $[Fe(THF)_6][Fe_4(N\text{-}p\text{-}Tol)_4(SDMP)_3(N\{SiMe_3\}_2)]_2$ ($[Fe(THF)_6][\mathbf{4}]_2$). The cubane oxidation state in **4** is reduced by one electron relative to **3** based on the presence of the known $[Fe(THF)_6]^{2+}$ dication[31] in the crystal lattice. A balanced reaction can be formulated via eq 2; application of this stoichiometry does result in the production of **4** at significant levels, although cluster type **3** remains the dominant product in about 2:1 ratio by ^{1}H NMR analysis.

$$9Fe(N\{SiMe_3\}_2)_2 + 6ArSH + 5Ar'NHNHAr' + \rightarrow Fe^{2+} + 2[Fe_4(NAr')_4(SAr)_3(N\{SiMe_3\}_2)]^- + 16HN(SiMe_3)_2 + Ar'N{=}NAr' \quad (2)$$

Crystal Structures. Dinuclear **2-THF** (Figure 1, Table 1) is an example of the well-precedented thiolate-bridged $[Fe_2(\mu\text{-}SR)_2]$ rhombic core geometry most commonly associated with terminal thiolate[32] or nitrosyl[33] ligation. A structural comparison of **2** against the close *p*-tolylthiolate analogue $Fe_2(S\text{-}p\text{-}Tol)_2(N\{SiMe_3\}_2)_2(THF)_2$ has been reported elsewhere,[29] where it was observed that the two core geometries differ in the nature of the rhombic distortion: in **2-THF**, the rhomb diagonal defined by the Fe···Fe separation is longer than the S···S diagonal, whereas the reverse is true for the tolyl derivative. This structural difference was attributed to a steric effect of the hindered mesityl substituent. We note here a further difference in the pyramidalization at sulfur, which is greater for the tolylthiolate dimer (∠Fe−S−C = 105.32(11), 107.66(12)° for tolyl, 114.07(8), 124.74(9)° for mesityl). This apparently induces a smaller Fe−S−Fe angle (81.74(3)° for tolyl, 94.45(2)° for mesityl), resulting in the reversed rhombic distortion compared to **2-THF**. In essence, the steric requirements of the ortho substituents on the mesityl group force a more planar 3-coordinate sulfur bridge, which opens the Fe−S−Fe angle as a consequence.

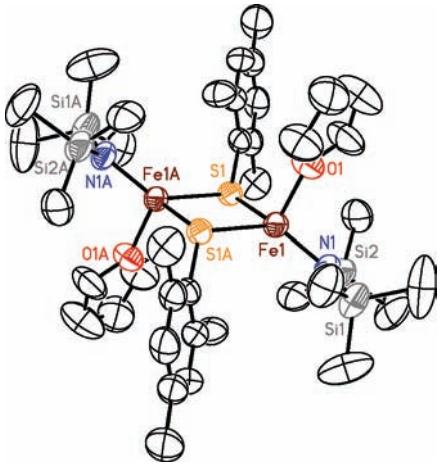

Figure 1. Structure of $Fe_2(SMes)_2(N\{SiMe_3\}_2)_2(THF)_2$ (**2-THF**), with thermal ellipsoids (50% probability level) and selected atom labels; hydrogen atoms are not shown. Labels ending in "A" indicate atoms related by crystallographic inversion symmetry.

Table 1. Selected Distances (Å) and Angles (deg) for $Fe_2(SMes)_2(N\{SiMe_3\}_2)_2(THF)_2$ (**2-THF**)

Fe1−S1	2.4294(7)	S1−Fe1−S1A	85.55(2)
Fe1−S1A	2.3847(7)	N1−Fe1−S1	119.31(7)
Fe1−N1	1.935(2)	N1−Fe1−S1A	135.00(7)
Fe1−O1	2.112(2)	O1−Fe1−S1	106.11(6)
Fe1···Fe1A	3.534(1)	O1−Fe1−S1A	101.04(6)
S1···S1A	3.270(1)	N1−Fe1−O1	106.02(9)
		Fe1−S1−Fe1A	94.45(2)

Clusters **3a** and **3b** possess the well-recognized $M_4Q_4L_4$ heterocubane geometry, in which Q is a μ_3 core ligand and L is a terminal ligand, and **4** is a site-differentiated derivative thereof (Figure 2, Tables 2 and 3). For **3a** and **3b**, three separate crystal structures, comprising six independent cluster molecules, have been determined. Across this set of observations, clusters either possess exact S_4 symmetry or can be idealized to approximate this symmetry, as dictated in particular by the disposition of thiolate substituents as shown in Figure 3. Deviations from perfect S_4 symmetry are associated primarily with canting of the aryl substituents. In all structures, imide and thiolate substituents associate in a pairwise stacking interaction of the aryl π faces; the closest C···C contacts within the paired aryl groups occur at approximately 3.5 Å, consistent with packing at van der Waals radii for aromatic carbons.[36] The mixed terminal ligand set in **4** forces lower symmetry and disrupts the intramolecular aryl stacking such that only two sets of thiolate/imide substituents are paired.

The $[Fe_4(NR)_4]^q$ core occurs elsewhere as chloride-ligated species $[Fe_4(N^tBu)_4Cl_4]^{0/1-}$[34] and $[Fe_4(NPh)_4Cl_4]^{2-}$.[35] In general, core geometries are largely equivalent between these different cluster classes. In comparison with the

(31) (a) Pohl, S.; Saak, W. *Z. Naturforsch. B* **1984**, *39*, 1236. (b) Saak, W.; Pohl, S. *Z. Anorg. Allg. Chem.* **1987**, *552*, 186. (c) Bolte, M.; Lerner, H.-W.; Scholz, S. *Acta Crystallogr., Sect. E* **2001**, *57*, m216.

(32) (a) Hagen, K. S.; Holm, R. H. *Inorg. Chem.* **1984**, *23*, 418. (b) Hauptmann, R.; Lackmann, J.; Chen, C.; Henkel, G. *Acta Crystallogr., Sect. C* **1999**, *55*, 1084. (c) Hauptmann, R.; Lackmann, J.; Henkel, G. *Z. Kristallogr.-New Cryst. Struct.* **1999**, *214*, 132. (d) Chen, C.; Hauptmann, R.; Lackmann, J.; Henkel, G. *Z. Kristallogr.-New Cryst. Struct.* **1999**, *214*, 137. (e) Henkel, G.; Chen, C. *Inorg. Chem.* **1993**, *32*, 1064. (f) Hammann, B.; Chen, C.; Florke, U.; Hauptmann, R.; Bill, E.; Sinnecker, S.; Henkel, G. *Angew. Chem., Int. Ed.* **2006**, *45*, 8245.

(33) (a) Harrop, T. C.; Song, D.; Lippard, S. J. *J. Am. Chem. Soc.* **2006**, *128*, 3528. (b) Tsou, C.-C.; Lu, T.-T.; Liaw, W.-F. *J. Am. Chem. Soc.* **2007**, *129*, 12626. (c) Chen, Y.-J.; Ku, W.-C.; Feng, L.-T.; Tsai, M.-L.; Hsieh, C.-H.; Hsu, W.-H.; Liaw, W.-F.; Hung, C.-H.; Chen, Y.-J. *J. Am. Chem. Soc.* **2008**, *130*, 10929. (d) Thomas, J. T.; Robertson, J. H.; Cox, E. G. *Acta Crystallogr.* **1958**, *11*, 599. (e) Lu, T.-T.; Tsou, C.-C.; Huang, H.-W.; Hsu, I.-J.; Chen, J.-M.; Kuo, T.-S.; Wang, Y.; Liaw, W.-F. *Inorg. Chem.* **2008**, *47*, 6040. (f) Harrop, T. C.; Song, D.; Lippard, S. J. *J. Inorg. Biochem.* **2007**, *101*, 1730. (g) Wang, R.; Camacho-Fernandez, M. A.; Xu, W.; Zhang, J.; Li, L. *Dalton Trans.* **2009**, 777.

(34) (a) Verma, A. K.; Nazif, T. M.; Achim, C.; Lee, S. C. *J. Am. Chem. Soc.* **2000**, *122*, 11013. (b) Link, H.; Decker, A.; Fenske, D. *Z. Anorg. Allg. Chem.* **2000**, *626*, 1567.

(35) Duncan, J. S.; Nazif, T. M.; Verma, A. K.; Lee, S. C. *Inorg. Chem.* **2003**, *43*, 1211.

(36) (a) Bondi, A. *J. Phys. Chem.* **1964**, *68*, 441. (b) Rowland, R. S.; Taylor, R. *J. Phys. Chem.* **1996**, *100*, 7384.

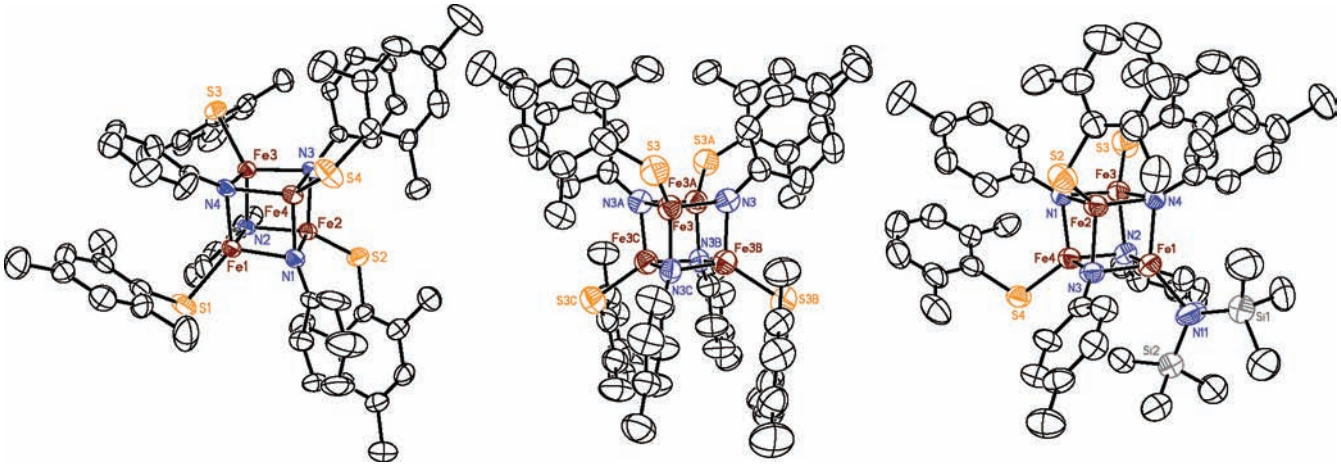

Figure 2. Structures of iron-arylimide cubane clusters $Fe_4(NPh)_4(SMes)_4$ (**3a**·1.5C_6H_6, left), $Fe_4(N\text{-}p\text{-}Tol)_4(SMes)_4$ (**3b**·0.5C_6H_6, tetragonal lattice, center), and $[Fe_4(N\text{-}p\text{-}Tol)_4(SDMB)_3N(SiMe_3)_2]^-$ ([$Fe(THF)_6$][**4**]$_2$·2THF, right), with thermal ellipsoids (50% probability level) and selected atom labels; hydrogen atoms are not shown. Two independent, complete clusters occur in the asymmetric unit of **3a**·1.5C_6H_6, of which one is shown above. In the asymmetric unit of tetragonal **3b**·0.5C_6H_6, three independent clusters exist, with two possessing crystallographic 4-fold rotoinversion symmetry and one having 2-fold rotational symmetry; one of the S_4-symmetric clusters is depicted above, with labels ending in "A", "B", or "C" indicating atoms related by imposed symmetry. A second, monoclinic form of **3b** is given as Supporting Information.

Table 2. Selected Distances (Å) and Angles (deg) for $Fe_4(NPh)_4(SMes)_4$·1.5C_6H_6 (**3a**·1.5C_6H_6), $Fe_4(N\text{-}p\text{-}Tol)_4(SMes)_4$·0.5$C_6H_6$ (**3b**·0.5C_6H_6), and $Fe_4(N\text{-}p\text{-}Tol)_4(SMes)_4$ (**3b**)[a]

	3a·1.5C_6H_6[a]			**3b**·0.5C_6H_6 (tetragonal lattice)[b]			**3b** (monoclinic lattice)		
	n[c]	mean[d] of n	range[e]	n[c]	mean[d] of n	range[e]	n[c]	mean[d] of n	range[e]
Fe−N	24	1.963(13)	1.940(5)−1.985(5)	12	1.962(13)	1.942(5)−1.983(5)	12	1.966(8)	1.953(2)−1.976(2)
Fe−S	8	2.214(9)	2.200(2)−2.225(2)	4	2.215(4)	2.209(2)−2.218(2)	4	2.215(11)	2.2044(9)−2.2275(9)
Fe···Fe	12	2.63(2)	2.5928(12)−2.6662(11)	8	2.62(2)	2.578(2)−2.6468(13)	6	2.63(3)	2.5712(6)−2.6445(6)
N···N	12	2.904(12)	2.886(7)−2.925(7)	8	2.91(2)	2.875(9)−2.956(9)	6	2.92(2)	2.899(3)−2.958(3)
N−Fe−N	24	95.4(7)	94.4(2)−97.1(2)	12	95.7(8)	94.6(2)−97.7(2)	12	95.8(10)	94.76(10)−98.29(10)
N−Fe−S	24	121(3)	114.55(15)−127.6(2)	12	121(3)	115.3(2)−127.5(2)	12	121(3)	115.67(7)−124.62(8)
Fe−N−Fe	24	84.3(6)	82.9(2)−85.2(2)	12	84.0(7)	82.2(2)−84.8(2)	12	83.8(9)	81.81(9)−84.51(9)
Fe_2N_2 planarity[f]	12	0.048(9)	0.036−0.063	8	0.049(12)	0.028−0.067	6	0.052(11)	0.036−0.060

[a] Asymmetric unit contains two independent, complete clusters. [b] Asymmetric unit contains two independent quarter-clusters (crystallographic S_4 symmetry) and a single half-cluster (crystallographic C_2 symmetry). [c] Number of independent observations of the metric type. [d] Arithmetic mean, with uncertainty representing the standard deviation from the mean. [e] Range of independent values. [f] rms displacement of the four rhomb atoms.

Table 3. Selected Distances (Å) and Angles (deg) for[$Fe(THF)_6$][$Fe_4(N\text{-}p\text{-}Tol)_4$-$(SDMP)_3(N\{SiMe_3\}_2)$]$_2$·2THF ([$Fe(THF)_6$][**4**]$_2$·2THF)

	n[a]	mean of n[b]	range[c]
Fe−N	12	1.98(3)	1.927(5)−2.034(5)
Fe−S	3	2.248(8)	2.242(2)−2.257(2)
Fe···Fe	6	2.66(8)	2.5929(13)−2.8113(13)
N···N	6	2.93(4)	2.853(7)−2.961(7)
N−Fe−N	12	95(3)	89.8(2)−97.7(2)
N−Fe−S	9	121(6)	113.0(2)−132.2(2)
Fe−N−Fe	12	84(2)	82.2(2)−89.0(2)
Fe_2N_2 planarity[d]	6	0.05(4)	0.019−0.102
Fe−N(amide)	1	1.940(6)	
N(amide)−Fe−N	3	122(9)	113.8(3)−132.2(2)
Fe−O(THF)	4	2.138(19)	2.117(6)−2.159(4)

[a] Number of independent observations of the metric type. [b] Arithmetic mean, with uncertainty representing the standard deviation from the mean. [c] Range of independent values. [d] rms displacement of the four rhomb atoms.

N^{t}Bu clusters, the present arylimide clusters exhibit slightly longer Fe−N bonds (0.03 Å) at the same all-ferric oxidation state; this appears to be an intrinsic difference associated with aryl versus alkyl substitution. In comparing arylimide species, the reduced cluster possesses longer Fe−N and Fe···Fe distances, consistent with the repulsive effect of increased charge.

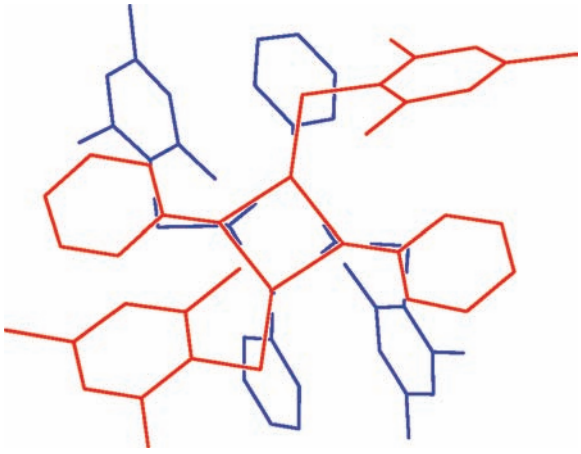

Figure 3. Projection along the pseudo-S_4 axis of the C_1-symmetric structure of $Fe_4(NPh)_4(SMes)_4$ (**3a**·1.5C_6H_6), illustrating the idealized S_4 cluster symmetry and the disposition of the aryl ligand substituents. For clarity, top and bottom halves of the cluster are depicted in red and blue, respectively.

The iron-imide (Fe-NR) cores of **3a**, **3b**, and **4** can also be compared with the [Fe_4S_4] cores that constitute the largest and most well-studied set of weak-field heterocubanes.[37] The core geometry of Fe_4S_4 clusters can be

Table 4. Spectroscopic Data

	electronic absorption:[a] λ, nm (ε_M, L·mol^{-1}·cm^{-1})	^{1}H NMR:[b] δ, ppm	Mössbauer:[c] δ ($\lvert\Delta E_Q\rvert$), mm/s
$Fe_2(SMes)_2(N\{SiMe_3\}_2)_2(THF)_2$ (**2-THF**)	255 (21,800), 285 (13,900)	THF-d_8: 15.7, 22.1, 23.6, 27.9, 33.0 (all v br); CD_3CN:[d] 1.8 (THF), 3.6 (THF), 15.4 (br, 18H, SiMe_3), 30.1 (br, 6H, *o-Me*), 34.3 (br, 2H, *m-H*), 39.4 (br, 3H, *p-Me*)	0.87 (1.84)
$Fe_4(NPh)_4(SMes)_4$ (**3a**)		−0.99 (br, 4H, Ph-*p-H*), 0.65 (br, 8H, Ph-*o-H*), 5.01 (12H, Mes-*p-Me*), 5.49 (br, 24H, Mes-*o-Me*), 11.77 (8H, Mes-*m-H*), 13.51 (8H, Ph-*m-H*)	
$Fe_4(N$-*p*-$Tol)_4(SMes)_4$ (**3b**)	240 (62,800), 455 (36,400)	1.8 (br, 8H, Tol-*o-H*), 4.47 (12H, Mes-*p-Me*), 5.40 (br, 24H, Mes-*o-Me*), 7.71 (12H, Tol-*p-Me*), 11.623 (8H, Mes-*m-H*), 12.91 (8H, Tol-*m-H*)	0.35 (0.70)
$[Fe(THF)_6][Fe_4(N$-*p*-$Tol)_4(SDMP)_3(N\{SiMe_3\}_2)]_2$ ($[Fe(THF)_6][$**4**$]_2$)	235 (128,000), 326 (63,900)[e]	−2.79 (br, 6H, Tol-*o-H*), 0.0 (br, 2H, Tol-*o-H*), 1.66 (br, 24H, Fe-THF-*β-H*), 1.96 (18H, SiMe3), 4.15 (br, 24H, Fe-THF-α-*H*), 5.27 (3H, DMP-*p-H*), 5.40 (18H, DMP-*o-Me*), 9.44 (3H, Tol-*p-Me*), 11.77 (6H, DMP-*m-H*), 12.75 (9H, Tol-*p-Me*), 13.24 (2H, Tol-*m-H*), 14.88 (6H, Tol-*m-H*)	

[a] THF solution, ca. 22 °C. [b] THF-d_8 and CD_3CN for **2-THF**, C_6D_6 solution for all others, ca. 22 °C. [c] Isomer shifts measured at 4.2 K, referenced to Fe metal at room temperature; errors in fit estimated at 0.02 mm/s. [d] The spectrum of crystalline **2-THF** in CD_3CN also shows an additional feature, an upfield shoulder to the $SiMe_3$ resonance at ca. 15% relative intensity; this signal appears to correspond to **1** in CD_3CN and can be eliminated by titration with additional MesSH. [e] Molar absorption coefficients reported per mole of cluster **4** to facilitate comparison with values for **3b**.

viewed as a polyhedron constructed from concentric interpenetrating Fe_4 and S_4 tetrahedra, with distinctly nonplanar Fe_2S_2 rhomb faces; S−Fe−S angles approach tetrahedral angles, but Fe−S−Fe angles are markedly acute (ca. 73°, on average). By comparison, the imide cubanes are more compact because of shorter Fe-Q bond lengths and also more cubic, with flatter Fe_2N_2 rhombs and rhomb interior angles that more closely approach 90°. Fe···Fe separations are slightly shorter in the imide system by about 0.1 Å. Assuming rigid Fe−Q bond lengths and factoring the difference in lengths, the structural observations suggest that nonbonded, repulsive interactions within the Fe_2Q_2 rhombs account for the angular differences. For the larger sulfide donor, a longer Q···Q separation is enforced, resulting in sharper Fe−Q−Fe angles. The smaller nitrogen donors allow closer Q···Q contacts, therefore more open Fe−Q−Fe angles, while repulsive Fe···Fe interactions prevent more open Q−Fe−Q angles.

At a finer level (deviations of ca. 0.03 Å for Fe−S distances), the cores of Fe_4S_4 clusters also exhibit slight, regular distortions away from idealized T_d symmetry, usually in the form of a D_{2d} distortion.[37] The $Fe_4(NR)_4$ cores show evidence of similar deformations, although the deviations are less internally consistent than those observed in the Fe−S cubanes. We note that the prominent interligand stacking interactions in the present system may affect core metrics, precluding the identification of subtle intrinsic core geometry preferences.

Physical Properties of Cubane Clusters. Spectroscopic data are compiled in Table 4.

In solution, cubane cluster types **3** and **4** are readily identified by their characteristic ^{1}H NMR spectra (Figure 4). All derivatives investigated show spectral patterns consistent with freely rotating ligand substituents and highest averaged point symmetry (T_d for **3**, C_{3v} for **4**), and resonances were completely assigned through a combination of relative peak areas, ^{1}H COSY, NOEDS, and ligand derivatization. Cluster paramagnetism generates isotropically shifted signals for the aryl substituents that alternate in displaced direction with alternant hydrocarbon position (downfield: *m*-H, *o*-Me, *p*-Me; upfield: *o*-H, *p*-H), implying a predominant spin polarization (delocalization) mechanism.[38]

Solution electronic absorption spectra of the Fe−NR cubane clusters display intense charge transfer bands in the near-UV-to-visible regions; comparative UV−vis spectra (including that of **2**) are presented in Figure 5. The all-ferric cubanes **3** show much more extensive absorption into the visible range of the spectrum in comparison with the one-electron reduced and ligand substituted cluster **4**, resulting in visually apparent color differences of maroon (**3a**, **3b**) versus brown (**4**). This is consistent with LMCT behavior upon replacement of a thiolate by an amide donor and upon reduction of core oxidation state, both of which destabilize further core reduction and shift LMCT transitions to higher energy.[39] Redox properties, however, could not be quantified directly; cyclic voltammetry revealed only broad, irreversible processes for **3a**, and no measurements were made on side product **4**.

In the solid state, zero-field ^{57}Fe Mössbauer measurement of polycrystalline **3b** reveals a single quadrupole doublet with isomer shift and quadrupole splitting consistent with high-spin Fe(III) and quite similar to those of the only other all-ferric Fe-NR cubane, $Fe_4(N^tBu)_4Cl_4$, characterized by Mössbauer spectroscopy.[34] Magnetic susceptibility measurements on **3b** reveal temperature-dependent susceptibility that decreases to a minimum with decreasing temperature (1.1 μ_B at 55 K) before rising at still lower temperatures (Figure 6). This behavior is well-known in Fe−S cubane systems and indicates a net diamagnetic cluster ground state in the presence of trace paramagnetic contamination.[39,40] Magnetically active,

(37) (a) Rao, P. V.; Holm, R. H. *Chem. Rev.* **2004**, *104*, 527. (b) Berg, J. M.; Holm, R. H. In *Iron-Sulfur Proteins*; Spiro, T. G., Ed.; Wiley: New York, 1982; Chapter 1.

(38) (a) Horrocks, W. D., Jr. Analysis of Isotropic Shifts. In *NMR of Paramagnetic Molecules: Principles and Applications*; LaMar, G. N., Horrocks, W. D., Jr., Holm, R. H., Eds.; Academic Press: New York, 1973; Chapter 4. (b) Holm, R. H.; Phillips, W. D.; Averill, B. A.; Mayerle, J. J.; Herskovitz, T. *J. Am. Chem. Soc.* **1974**, *96*, 2109.

(39) Sharp, C. R.; Duncan, J. S.; Lee, S. C. *Inorg. Chem.* **2010**, *49*, 6697.

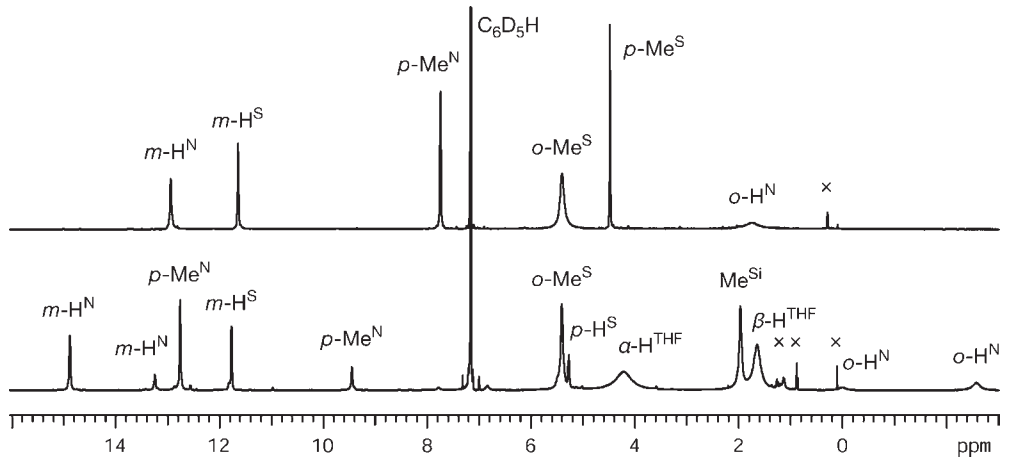

Figure 4. ^{1}H NMR spectra (C_6D_6, 500 MHz, 295 K) of $Fe_4(N\text{-}p\text{-}Tol)_4(SMes)_4$ (**3b**, top), and $[Fe(THF)_6][Fe_4(N\text{-}p\text{-}Tol)_4(SDMB)_3N(SiMe_3)_2]_2$ ($[Fe(THF)_6][\mathbf{4}]_2$, bottom). Resonances are labeled with superscripts indicating ligand type (N = imide, S = thiolate) and x = trace diamagnetic contaminants (solvent or silylmethyl-containing species).

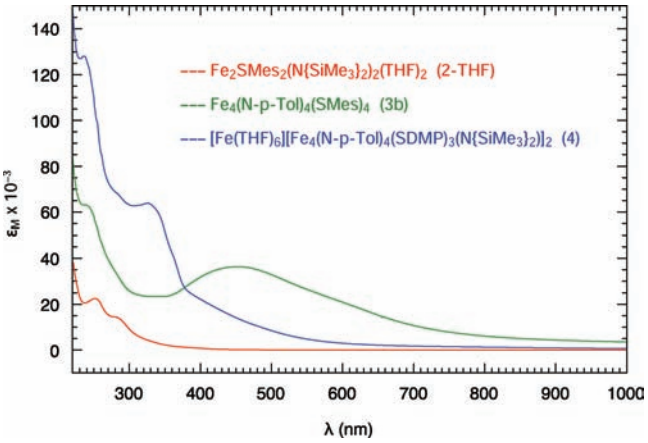

Figure 5. UV−visible absorption spectra of $Fe_2(SMes)_2(N\{SiMe_3\}_2)_2(THF)_2$ (**2-THF**), $Fe_4(N\text{-}p\text{-}Tol)_4(SMes)_4$ (**3b**), and $[Fe(THF)_6][Fe_4(N\text{-}p\text{-}Tol)_4(SDMB)_3N(SiMe_3)_2]_2$ ($[Fe(THF)_6][\mathbf{4}]_2$) in THF. The spectrum of **2-THF** (1.0 mM) cannot be associated definitively with the solid-state structure because of possible speciation in solution. The molar absorptivity of $[Fe(THF)_6][\mathbf{4}]_2$ is normalized per cubane cluster.

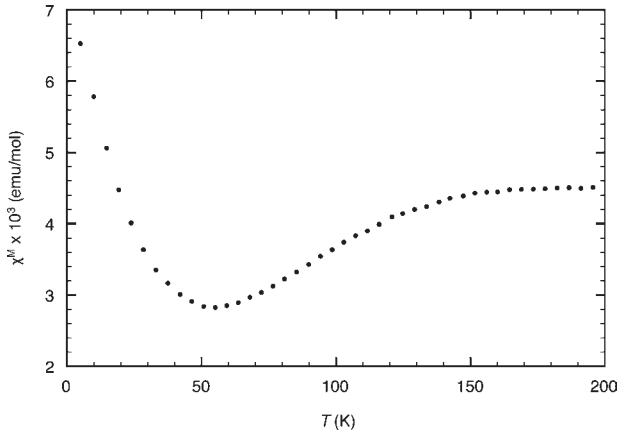

Figure 6. Temperature dependence plot of the molar magnetic susceptibility of polycrystalline $Fe_4(N\text{-}p\text{-}Tol)_4(SMes)_4$ (**3b**).

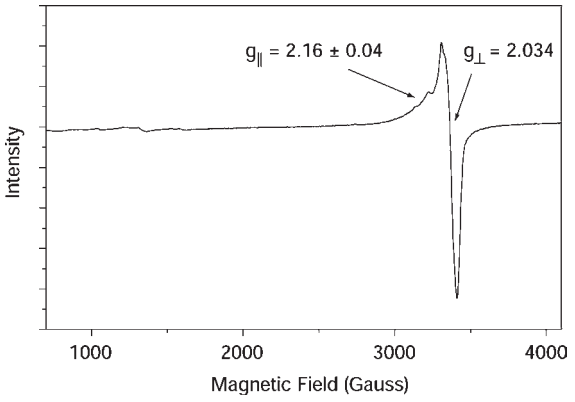

Figure 7. Perpendicular mode EPR spectrum of $[Fe(THF)_6][Fe_4(N\text{-}p\text{-}Tol)_4(SDMB)_3N(SiMe_3)_2]_2$ ($[Fe(THF)_6][\mathbf{4}]_2$) (12 K, frozen toluene glass), with axial signal features indicated.

but spectroscopically silent, impurities are persistent in this system and must be minimized by careful recrystallization; indeed, our earlier magnetic measurements and spin state assignment for cluster **3a** (originally reported as a $S = 2$ ground state) are probably in error because of magnetic contaminants.[26] For cluster **4**, zero-field Mössbauer measurement yielded broad absorptions that could not be reliably fitted, and magnetochemical studies were not attempted. The electron paramagnetic resonance (EPR) spectrum of **4a** at 12 K in frozen toluene glass (Figure 7) shows an axial signal pattern with $g = 2.034$, 2.16(4) that is consistent with a $S = 1/2$ ground state.

N−N Bond Reduction: Mechanism and Scope. Given the reaction stoichiometry proposed in eq 1 and the dinuclear solid-state structures of precursors **1**[27b] and **2-THF**, it is tempting to propose that cluster assembly proceeds via the simple three-step sequence outlined in Scheme 2. This mechanism assumes tetrahedral, 4-coordinated Fe(II/III) environments and the intermediacy of bridged dinuclear species. The reaction begins with protolysis of the latent amide base in **2** and concomitant formation of a μ:η^2,η^2 hydrazide(2−)-bridged dimer. Reductive scission of the

(40) (a) Laskowski, E. J.; Frankel, R. B.; Gillum, W. O.; Papaefthymiaou, G. C.; Renaud, J.; Ibers, J. A.; Holm, R. H. *J. Am. Chem. Soc.* **1978**, *100*, 5322. (b) Herskovitz, T.; Averill, B. A.; Holm, R. H.; Ibers, J. A.; Phillips, W. D.; Weiher, J. F. *Proc. Natl. Acad. Sci. U.S.A.* **1972**, *69*, 2437. (c) Cleland, W. E.; Holtman, D. A.; Sabat, M.; Ibers, J. A.; DeFotis, G. C.; Averill, B. A. *J. Am. Chem. Soc.* **1983**, *105*, 6021.

Scheme 2[a]

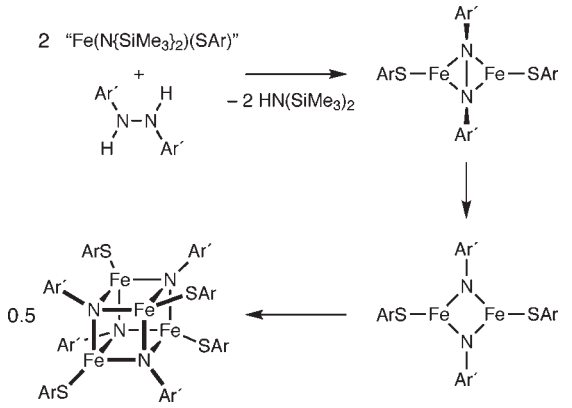

[a] **Note: The 3-coordinate iron centers are notional; solvent coordination or bridging interactions to give 4-coordinate iron are likely.**

Table 5. Reactivity of **2** (2 equiv) with N−N/N=N Substrates (1 equiv)

substrate	products[a] (% yield)
PhHN−NHPh	PhNHBz (47), PhN=NPh (18)
(*p*-Tol)HN−NH(*p*-Tol)	(*p*-Tol)NHBz (55), (*p*-Tol)N=N(*p*-Tol) (18)
PhHN−N(Me)Ph	**3** and other clusters[b]
Ph(Me)N−N(Me)Ph	no reaction
^{i}PrHN−NH^{i}Pr	^{i}PrNHBz (13), ^{i}Pr(Bz)N−NHBz (38)
^{t}BuHN−NH^{t}Bu	no reaction
PhN=NPh	no reaction
H_2N-NH_2	H_2NBz (5)

[a] Characterized by GC assay following acidification/extraction/benzoylation protocol unless otherwise indicated. All peaks in the chromatograms were identified, including thiolate-derived species (MesSH, MesSSMes, MesSBz), BzOH, and BzOBz; only substrate-derived products are reported. [b] Identified by NMR assay of crude reaction mixture.

N−N bond coupled with simultaneous 2-electron oxidation of the two ferrous centers gives a diferric diimide dimer as the next step. Finally, fragment condensation of two diimide dimers yields the ultimate cubane product. The feasibility of the final step has been demonstrated and is discussed elsewhere as a separate report;[41] we address here the chemistry of N−N bond reduction. We do not exclude the possibility of alternate, non-concerted, one-electron mechanisms in this chemistry; Scheme 2 merely offers a simple starting hypothesis for consideration.

The coupling of hydrazine N−N bond reduction with oxidation of Fe(II) to Fe(III) in dinuclear complexes per Scheme 2 has been invoked in a dinuclear cyclopentadienyl-ligated system[23] and, very recently, observed as a direct transformation in a triphosphinoborate-ligated complex.[21b] In the present system, mechanistic investigation is hindered by factors intrinsic to weak-field cluster self-assembly chemistry. The weak-field, 4-coordinate iron sites are exchange-labile and undergo substantial, rapid reorganization over the course of product formation. Solution spectroscopic compound identification is challenging without prior physical isolation and structural characterization, and paramagnetic line broadening increases the difficulty in detecting low-concentration species. In general, the direct tracking of a reaction sequence is not possible under these conditions. Operating within these constraints, we offer the following observations based on test reactions of **2** (2 equiv) with various hydrazines (1 equiv) in benzene, with reaction assays summarized in Table 5.

(a) Mass Balance and Azoarene Formation. The formation of significant quantities of azoarenes in the synthesis of **3** requires explanation, particularly as the reaction stoichiometry proposed in eq 1 does not produce azoarene. Hydrazine disproportionation (eq 3) is one potential source of diazenes; this reaction displays no net metal-based redox changes and appears to be the primary mechanism of N−N bond reduction in several iron-mediated reaction systems.[21a,24]

$$2\mathrm{PhNHNHPh} \rightarrow 2\mathrm{PhNH_2} + \mathrm{PhN{=}NPh} \qquad (3)$$

To probe the relationship of azoarene formation to N−N bond reduction in the present system, we endeavored to quantitate the mass balance following cluster assembly. NMR spectroscopic analysis of the crude reaction mixtures was found to be inadequate for this purpose because of ill-defined, magnetically active contaminants that broadened resonances and precluded accurate signal integration. Instead, organic products were identified and quantified by gas chromatographic analysis following acid digestion to release metal-bound moieties and derivatization (benzoylation[42]) to detectable analytes.

Analyses of the reactions with 1,2-Ar′NHNHAr′ give 47 and 55% Ar′NHBz (benzoylated arylamine) for Ar′ = Ph and *p*-Tol, respectively, and 18% Ar′N=NAr′ (for either aryl group) based on initial hydrazine nitrogen content, with no other arylnitrogen species detected. The total recovery of diarylhydrazine-derived species is about 70%, which is similar to recoveries from control assays under equivalent conditions (ca. 80% maximum, see Experimental Section); we therefore believe these results accurately reflect the distribution of arylnitrogen-containing species in the crude reaction systems. These assays indicate that about 75% of the hydrazine is reduced and 25% is oxidized. This immediately excludes disproportionation as the primary pathway for N−N bond reduction, inasmuch as eq 3 can only explain one-third of the reduced nitrogen content based on azoarene yields.

Nonetheless, we believe that disproportionation does contribute to the product distribution. The product heterocubane clusters **3a** and **3b**, or unidentified species derived therefrom, catalyze the disproportionation of 1,2-diarylhydrazines to arylamines and azoarenes. Disproportionation is evident and effective at low cluster loadings (0.1 mol % vs hydrazine), and the reaction is complete within minutes at cluster and hydrazine concentrations similar to actual preparative conditions. Azoarenes themselves are unreactive with the species in this system. We have observed facile, catalytic diarylhydrazine disproportionation in an unrelated ferrous thiolate system;[43] these findings, along with other documented roles in Fe-mediated hydrazine reduction chemistry,[21a,24] suggest that disproportionation is a common reactivity mode. If we attribute all azoarene formation to this catalytic process, thereby accounting for one-third of the reduced nitrogen content, and we assume eq 1 as the operative pathway that

(41) Zdilla, M. J.; Lee, S. C., manuscript in preparation.

(42) Barreira, E. S.; Parente, J. P.; Wilson de Alencar, J.. *J. Chromatogr.* **1987**, *398*, 381.

(43) Zdilla, M. J.; Verma, A. K.; Lee, S. C. *Inorg. Chem.* **2008**, *47*, 11382.

generates the remainder of the reduced nitrogen, we expect a 50% maximum yield of cubane **3**, which is comparable to the actual crude isolated yields.

The other product formed in this system is a black, benzene-insoluble powder. ^{1}H NMR analysis of this material in THF-d_8 reveals broad, weak signals indicative of paramagnetic material but is otherwise uninformative. Acid digestion/benzoylation/GC assay of the Ar′ = Ph reaction shows the presence of mesitylthiolate-derived analytes (MesSH, MesSBz, $(MesS)_2$) at 14% total yield, as well as low levels of PhNHBz (3%), indicating that the material is predominantly iron-thiolate in composition.

(b) [NAr] Crossover. A crossover experiment involving the reaction of a 1:1 mixture of 1,2-diphenylhydrazine and 1,2-di-*p*-tolylhydrazine (at 1 equiv of total hydrazine content) was conducted to obtain evidence of the concerted dinuclear mechanism proposed in Scheme 2. The detection of a mixed imide $Fe_4(NPh)_n(N\text{-}p\text{-}Tol)_{n-4}(SMes)_4$ cubane distribution favoring $n = 0$, 2, and 4 congeners would support this mechanism. Instead, extensive core mixing is observed, with essentially statistical distributions of all possible cluster core compositions. This result is inconclusive, however, as the production of arylamine via disproportionation (eq 3) gives rise to a side reaction, specifically the rapid exchange of core imides with free amines (eq 4). The details of this core exchange chemistry and full spectroscopic assignments are described in a separate report.[41] We note that azoarenes obtained in this crossover experiment, as well as in catalytic disproportionation assays involving mixed hydrazines, are almost exclusively (90−95%) symmetric by GC/MS analysis, strongly suggesting that azoarene does not arise from separated ArN fragments; the low levels of mixed azoarene product probably originate from the oxidation of reduced arylnitrogen species during the aerobic workup prior to GC analysis.

$$Fe_4(NAr')_4(SAr)_4 + Ar^*NH_2 \rightarrow Fe_4(NAr^*)_n(NAr')_{4-n}(SAr)_4 \qquad (n = 0-4) \tag{4}$$

(c) Scope of N−N Bond Reduction. Other hydrazines were surveyed to delineate the extent of N−N reduction chemistry. Tetrasubstituted PhMeN−NMePh is unreactive, while trisubstituted PhMeN−NHPh leads to a dark solution that reveals, by ^{1}H NMR analysis, a complex array of isotropically shifted resonances characteristic of paramagnetic cluster species, including the signal sets for **3a** and the (NPh,SMes)-derivative of **4**. These results suggest that N−H deprotonation is necessary for N−N bond reduction in this system and that a single deprotonation to hydrazide(1−) is sufficient to achieve this. Perhaps the formation of a dinuclear N−bridging interaction facilitates the reduction of the N−N bond by organizing a 2-electron reduction from 1-electron Fe(II) reductants; deprotonation of the substrate to the nitrogen anion form would favor N-bridging. No azoarene is detected in the trisubstituted hydrazine system, consistent with the conclusions from the mass balance and crossover experiments that argue against a direct role for hydrazine disproportionation in the formation of the cubane clusters.

Parent and alkyl-substituted hydrazines were also tested for reactivity. Not all substrates are reactive, but those that are give black product mixtures visually similar to the arylhydrazine reaction systems. The dark solids isolated from these reactions, however, proved difficult to characterize, with poor solubility in benzene and no diagnostic NMR signals in THF-d_8 solution.

Parent hydrazine reacts to form a black reaction mixture within 5 min. Analysis of the crude reaction mixture by either acid digestion/benzoylation/GC or spectroscopic indophenol assay[44] confirm the presence of ammonia in low yield (5% based on total N_2H_4 and $[N(SiMe_3)_2]^-$ nitrogen content). This recovery is too low to interpret, especially as silylamide hydrolysis provides an additional source of reduced nitrogen. It is possible that ammonia is lost during our workup protocol, that reduced nitrogen is trapped as insoluble iron-containing precipitate, or that N_2H_4 functions as a reductant in this system, with release of N_2 and formation of reduced iron.

1,2-Diisopropylhydrazine reacts at diminished rates relative to the reactions with 1,2-diarylhydrazines (darkening to opacity in ca. 45 min vs immediate). Assay of the crude reaction mixture by benzoylation/GC analysis reveals that 13% of the nitrogen originates from N−N bond cleavage, while 38% of the nitrogen content appears in the form of ^{i}PrBzNNHBz; azo-isopropane, if present, was not detected because of its low boiling point. The recovery of unreduced hydrazine with a missing isopropyl substituent indicates the existence of an alternate reaction path. Although the fate of the alkyl group is uncertain, one possibility is hydrogen elimination at the α-position to form a hydrazone, which hydrolyzes upon acidic aqueous workup (eq 5) to give, after derivatization, the final analyte. Similar behavior has been observed in other Fe-NR cluster systems and has precluded preparation of iron-alkylimide clusters with hydrogens at positions α to nitrogen.[45]

$$^i\text{PrHNN}{=}\text{CMe}_2 + H_2O \rightarrow {}^i\text{PrNHNH}_2 + \text{Me}_2\text{C}{=}\text{O} \tag{5}$$

Hydrazine sterics also appear to influence the reactivity. Thus, 1,2-diethylhydrazine reacts in a qualitatively similar fashion to 1,2-diisopropylhydrazine, although at a faster rate (ca. 30 s); product analysis was not attempted on this system because of the volatility of the ethylamine product prior to derivatization. 1,2-Di-*t*-butylhydrazine, by contrast, shows no color change when mixed with **2**, although a small quantity of light-colored precipitate is observed. ^{1}H NMR analysis suggests the formation of a weak adduct in C_6D_6 based on the appearance of new, sharp, isotropically shifted resonances; addition of THF, however, returns crystalline **2** in quantitative yield. The absence of reactivity for this hydrazine likely arises from the congested steric environment about the N−N bond, which may hinder adoption of ligand geometries necessary for N−N bond scission.

Summary and Implications

Ferrous amide thiolate species can react with 1,2-diarylhydrazines to form iron-arylimide-thiolate cubanes. The imide

(44) Chaney, A. L.; Marbach, E. P. *Clin. Chem.* **1962**, *8*, 130.
(45) Duncan, J. S.; Zdilla, M. J.; Lee, S. C. *Inorg. Chem.* **2007**, *46*, 1071.

ligands arise from the 2-electron reduction of the hydrazine N−N bond, through a transformation that appears to be coupled to the 1-electron oxidation of Fe(II) to Fe(III). Although reactivity is evident with a number of different thiolate ligands and hydrazine substrates, well-defined iron-containing products (cubane clusters, exclusively) are found only from the specific combination of sterically hindered arylthiolate ligands and 1,2-diarylhydrazines. Analysis of the organic products reveals behavior that is variable and substrate-dependent, with catalytic hydrazine disproportionation and organohydrazine N−C bond cleavage also observed under appropriate conditions. These results establish that simple N−N bond reduction is but one of several possible reactivity modes available in the reaction of simple iron precursors with hydrazines.

Observations derived from synthetic systems can only be extrapolated to N−N bond reduction in nitrogenases with caution. At present, the enzyme systems provide limited information on reactive states, synthetic complexes mimic the FeMo-cofactor environment incompletely at best, and iron-hydrazine reaction chemistry is demonstrably complex. Under these circumstances, synthetic results only outline chemical possibilities. In previous studies of synthetic weak-field iron−sulfur environments, parent and alkyl-substituted hydrazines were found inert to reaction chemistry beyond simple N-coordination using low-coordinate ferrous thiolate[42] or $[Fe_4S_4(SR)_4]^{2-}$[12] species under aprotic or reducing/weakly protonating conditions; electrochemical reductions in protic solvents, however, have been noted.[13] For arylhydrazines, N−N bond cleavage from disproportionation or rearrangement reactions has been documented with ferrous thiolate[42] and diferrous sulfide-bridged β-diketiminate[24b] complexes in aprotic solvents. The present study expands the known chemistry, with N−N bond reduction proven in both aryl- and alkylhydrazines; activation via hydrazine deprotonation appears important in achieving this reactivity. Speculatively, these observations seem to fit with the limited activity of the nitrogenase enzymes for exogenous hydrazine substrate, although access to the reaction pocket and selective delivery of protons may be the limiting factors in the enzymatic reduction.[5,6] Partially reduced, anionic dinitrogen intermediates, that is, ligated hydrazides, are expected to undergo N−N cleavage chemistry readily in weak-field ferrous environments.

Experimental Section

General Considerations. All manipulations were conducted at room temperature under a pure dinitrogen atmosphere unless otherwise indicated. Previously described anaerobic synthetic and characterization (^{1}H NMR, UV−vis, Mössbauer, EPR spectroscopies; magnetic susceptibility measurement; elemental analysis) protocols[35,45] were used in the present study. 1,2-Diisopropylhydrazine,[46] isopropylhydrazine hydrochloride,[46] 1,2-di-*t*-butylhydrazine,[47] 1,2-di-*p*-tolylhydrazine,[48] 1-methyl-1,2-diphenylhydrazine,[49] 1-methyl-1,2-di-*p*-tolylhydrazine,[49] and 1,2-dimethyl-1,2-diphenylhydrazine[49] were prepared by literature methods. 1,2-Diethylhydrazine was obtained from the commercially available dihydrochloride salt (Aldrich) by treatment with excess 40% aqueous KOH, followed by extraction with CH_2Cl_2, preliminary drying over KOH, and final distillation from CaH_2. $Fe(N\{SiMe_3\}_2)_2$ (**1**) was synthesized by the procedure of Anderson et al,[27a] using $FeCl_2$ in place of $FeBr_2(THF)_2$.[50] All other chemicals were obtained from commercial sources or prepared as described below.

$Fe_2(\mu$-SMes$)_2(N\{SiMe_3\}_2)_2(THF)_2$ (2-THF). A clear solution of MesSH (0.304 g, 2.00 mmol) in THF (10 mL) was added to a stirred blue solution of **1** (0.753 g, 2.00 mmol) in THF (10 mL) to afford a color change from blue to red-brown. The reaction mixture was stirred 30 min and concentrated in vacuo to 10 mL, at which point yellow microcrystals were observed on the sides of the flask. To this mixture, 10 mL of *n*-pentane was added, crystallizing more material. The mixture was held at −30 °C for 20 min, then filtered to give 0.396 g of yellow microcrystalline **2** (0.450 mmol, 45%). Anal. Calcd for $C_{38}H_{74}O_2N_2S_2Si_4Fe_2$: C, 51.91; H, 8.48; N, 3.19. Found: C, 51.54; H, 8.52; N, 3.14.

$Fe_4(\mu_3$-NPh$)_4$(SMes$)_4$ (3a). MeSH (0.405 g, 2.66 mmol) in 10 mL of benzene was added dropwise over the course of 5 min to a stirred green solution of **1** (0.753 g, 2.0 mmol) in 10 mL of benzene to afford a brown solution with a brown precipitate, which dissolved upon further stirring for 10 min. To this brown solution, *N*,*N*′-diphenylhydrazine (0.245 g, 1.33 mmol) in 10 mL of benzene was added, resulting in an immediate color change to black. The reaction was stirred for 20 h, filtered to remove benzene-insoluble black powder, concentrated in vacuo to 5 mL, and diluted with 30 mL of hexamethyldisiloxane to give black microcrystalline material. The mixture was chilled for 20 min at −30 °C and filtered to isolate 0.193 g of black microcrystals. This first crop is contaminated by small amounts of NMR-silent, paramagnetic impurities based on NMR, magnetochemical, and elemental analyses. Product of improved purity was obtained from the filtrate following the initial crop by evaporation in vacuo to a total solution volume of 1−3 mL and storage for 1−2 days at −30 °C. The black crystals that result were isolated and dried (0.180 g, 0.151 mmol, 22.7%; total crude yield, including first crop: 47%). Anal. Calcd for $C_{60}H_{64}N_4S_4Fe_4$: C, 60.42; H, 5.41; N, 4.70. Found: C, 59.86; H, 4.93; N, 4.50.

$Fe_4(\mu_3$-N-*p*-Tol$)_4$(SMes$)_4$ (3b). A procedure analogous to the preparation of **3a** was followed using MesSH (0.304 g, 2.00 mmol, in 10 mL of benzene), **1** (0.753 g, 2.00 mmol, in 10 mL of benzene), and *N*,*N*′-di-*p*-tolylhydrazine (0.213 g, 1.00 mmol in 10 mL of benzene). After the first filtration to remove benzene-insoluble black powder, the filtrate was concentrated in vacuo to 3 mL and treated with 15 mL of pentane to give black microcrystals. The mixture was held at −30 °C for 20 min, then filtered to yield 0.256 g of black microcrystalline **3b** (0.199 mmol, 40% crude yield). Analytically pure samples were obtained by recrystallization of the initial microcrystalline product via *n*-pentane/benzene vapor diffusion at room temperature as follows: 50 mg of crude **3b** was dissolved in 0.4 mL of benzene, into which 2 mL of *n*-pentane was diffused; after 10 d, the supernatant was decanted, and the crystals rinsed with cold *n*-pentane to give 27 mg of pure crystalline **3b** (54% recovery to give 22% overall yield). Anal. Calcd for $C_{64}H_{72}N_4S_4Fe_4 \cdot 0.5C_6H_6$; C, 62.48; H, 5.87; N, 4.35. Found: C, 62.41; H, 5.94; N, 4.32.

$[Fe(THF)_6][Fe_4(\mu_3$-N-*p*-Tol$)_4$(SDMB$)_3N(SiMe_3)_2]_2$ ($[Fe(THF)_6]$-$[4]_2$). A procedure analogous to the preparation of **3a** was followed using 2,6-dimethylbenzenethiol (DMBSH; 0.185 g, 1.34 mmol, in 10 mL of benzene), **1** (0.753 g, 2.00 mmol, in 10 mL of benzene), and *N*,*N*′-di-*p*-tolylhydrazine (0.236 g, 1.11 mmol in 10 mL of benzene). The black reaction mixture was stirred for 20 h, then concentrated in vacuo to 5 mL, diluted with 15 mL of *n*-pentane, chilled for 20 min at −30 °C, and filtered to give 0.060 g of black powder, which contained **4** contaminated with substantial amounts of SDMB-ligated **3**. The filtrate was

(46) Ghali, N. I.; Venton, D. L.; Hung, S. C.; Le Breton, G. C. *J. Org. Chem.* **1981**, *46*, 5413.
(47) Stowell, J. C. *J. Org. Chem.* **1967**, *32*, 2360.
(48) Carlin, R. B.; Wich, G. S. *J. Am. Chem. Soc.* **1958**, *80*, 4023.
(49) Katritzky, A. R.; Wu, J.; Verin, S. V. *Synthesis* **1995**, 651.

(50) The presence of THF in the reaction system can lead to THF contamination in the final distilled product; details are provided as Supporting Information.

dried in vacuo to give 0.279 g of black powder. This powder was recrystallized by vapor diffusion of *n*-pentane/THF at −30 °C. After 60 h, black crystals were isolated, washed with cold (−30 °C) *n*-pentane, and dried in vacuo to give 0.070 g of **4** (0.02 mmol, 10%). Anal. Calcd for $C_{140}H_{194}N_{10}O_6S_6Si_4Fe_9 \cdot 2C_4H_8O$: C, 58.00; H, 6.91; N, 4.57. Found: C, 58.42; H, 6.56; N, 4.08.

Other $[Fe_4(\mu_3\text{-}NAr')_4(SAr)_3(N\{SiMe_3\}_2)]^-$ Cubanes. In our efforts to identify the cluster type represented by **4**, the following derivatives were also prepared: $[Fe_4(\mu_3\text{-}NPh)_4(SMes)_3(N\{SiMe_3\}_2)]^-$, $[Fe_4(\mu_3\text{-}N\text{-}p\text{-}Tol)_4(SMes)_3(N\{SiMe_3\}_2)]^-$, $[Fe_4(\mu_3\text{-}NPh)_4(SDMB)_3(N\{SiMe_3\}_2)]^-$. These derivatives were synthesized by appropriate combination of thiol and 1,2-diarylhydrazine per the synthesis of **4**, although the isolation of highly crystalline products in these cases proved problematic. By comparison with the spectrum of **4**, ^{1}H NMR data unambiguously identify the cluster type in the derivatives and are provided for reference as Supporting Information.

Gas Chromatographic Analysis. GC data were obtained using an Agilent 6850 Series GC system equipped with a flame ionization detector and a J&W Scientific HP-1 capillary column (dimethylpolysiloxane, 30 m length ×0.32 mm i.d. × 25 μm film). The injection chamber was held at 260 °C, He carrier gas delivered at 27.71 PSI at a flow rate of 4.5 mL/min, and the oven temperature program set to an initial temperature of 70 °C, ramping at 10 °C/min for 8 min, holding at 150 °C for 2 min, ramping at 20 °C/min for 5 min, and holding at a final temperature of 250 °C for 2 min.

Table 6. Extraction and Derivatization Control Assays

substrate	additional components	products (% yield)
^{i}PrNH$_2$		^{i}PrNHBz (82)
^{i}PrNH$_2$	$FeCl_2$	^{i}PrNHBz (40)
^{i}PrNH$_2$	$FeCl_3$	^{i}PrNHBz (70)
^{i}PrNH$_2$	$FeCl_2$ + Na_2EDTA	^{i}PrNHBz (75)
^{i}PrHN−NH^{i}Pr	$FeCl_2$ + Na_2EDTA	^{i}Pr(Bz)N−NH^{i}Pr (82), ^{i}Pr(Bz)N−N(Bz)^{i}Pr (2), ^{i}PrNHBz (4)
^{i}PrHN−NH^{i}Pr	$FeCl_3$ + Na_2EDTA	^{i}Pr(Bz)N−NH^{i}Pr (82), ^{i}Pr(Bz)N−N(Bz)^{i}Pr (2), ^{i}PrNHBz (5)
PhN=NPh		PhN=NPh (86)
PhN=NPh	$FeCl_2$	PhN=NPh (71)
PhN=NPh	$FeCl_3$	PhN=NPh (87)
$HN(SiMe_3)_2$	$FeCl_2$ or $FeCl_3$ + Na_2EDTA	$BzNH_2$ (1−33)[a]

[a] Recoveries of benzamide via the benzoylation protocol varied but were typically less than 5%.

(a) GC Assay for Fe-Mediated Hydrazine Reactivity. The organic products of the reaction between **2** and various hydrazines were separated and analyzed as follows. Under anaerobic conditions, MesSH (0.021 g, 0.20 mmol) in 2 mL of benzene was added dropwise to a stirred green solution of **1** (0.076 g, 0.20 mmol) in 2 mL of benzene, affording a color change to brown. After stirring for 5 min, 0.10 mmol of hydrazine (neat for diisopropylhydrazine, dissolved in 1 mL of benzene for diarylhydrazines) was added, darkening the solution color to black (immediate for aryl hydrazines, over the course of 45 min for diisopropylhydrazine). After 30 h, the reaction vessel was opened to air, and 5 mL of 6 M HCl added to liberate ligands from iron by protonolysis. The bilayer was mixed by vigorous stirring for 2 h, then partitioned.

The benzene layer, which contained neutral organic species (e.g., MesSH, $(MesS)_2$, azo compounds), was rinsed with 1 mL of 6 M HCl, partitioned, and dried over anhydrous Na_2SO_4. After filtration, a known quantity of internal integration standard (benzophenone or anthracene, typically 30 mg) was added, and the solution contents analyzed by GC.

The acidic aqueous fractions contained primarily iron, ammonium, and hydrazonium salts, with trace amounts of MesSH. These fractions were combined, chilled in an ice bath, and treated with Na_2EDTA to sequester iron, resulting in a white precipitate. The solution was made basic to litmus by dropwise addition of 5 M NaOH with mixing, resulting in dissolution of the white precipitate. To allow analysis of low-boiling components and assist in extractive separation of reaction products, the organic species were derivatized by benzoylation,[42] via the addition of 0.25 g $NaHCO_3$, followed by 0.1 mL of benzoyl chloride; for the di-*p*-tolylhydrazine system, 1 mL of CH_2Cl_2 was also added to dissolve precipitated *p*-toluidine. The reaction vessel was then sealed, stirred vigorously for 2 h, and extracted with 3 × 4 mL portions of CH_2Cl_2 to isolate the benzoylated products. The organic fractions were combined and dried for 5 min over anhydrous Na_2SO_4. After filtration, a known quantity of internal integration standard (benzophenone or anthracene, typically ca. 5 mg) was added, and the solution contents analyzed by GC. Retention times were compared with authentic reference compounds as prepared below, and yields were determined by comparison of peak integrals with internal standards.

Table 7. Crystallographic Data for $Fe_2(SMes)_2(N\{SiMe_3\}_2)_2(THF)_2$ (**2-THF**), $Fe_4(NPh)_4(SMes)_4 \cdot 1.5C_6H_6$ (**3a**$\cdot 1.5C_6H_6$), $Fe_4(N\text{-}p\text{-}Tol)_4(SMes)_4 \cdot 0.5C_6H_6$ (**3b**$\cdot 0.5C_6H_6$), $Fe_4(N\text{-}p\text{-}Tol)_4(SMes)_4$ (**3b**), and $[Fe(THF)_6][Fe_4(N\text{-}p\text{-}Tol)_4(SDMP)_3(N\{SiMe_3\}_2)]_2 \cdot 2THF$ ($[Fe(THF)_6][\mathbf{4}]_2 \cdot 2THF$)[a]

	2-THF	**3a**$\cdot 1.5(C_6H_6)$	**3b**$\cdot 0.5C_6H_6$	**3b**	$[Fe(THF)_6][\mathbf{4}]_2 \cdot 2THF$
formula	$C_{38}H_{74}Fe_2N_2O2S_2Si_4$	$C_{69}H_{73}Fe_4N_4S_4$	$C_{67}H_{75}Fe_4N_4S_4$	$C_{64}H_{72}Fe_4N_4S_4$	$C_{148}H_{210}Fe_9N_{10}O_8S_6Si_4$
fw	879.17	1309.96	1287.95	1248.90	3064.63
space group	$P\bar{1}$ (no. 2)	$P\bar{1}$ (no. 2)	$P\bar{4}n2$ (no. 118)	$P2_1/c$ (no. 14)	$C2/c$ (no. 15)
Z	1	4	8	4	4
a, Å	10.4231(3)	15.2729(7)	17.1488(8)	20.7971(5)	25.5272(5)
b, Å	10.9167(5)	18.6174(7)	17.1488(8)	11.4905(3)	21.9314(5)
c, Å	12.8489(5)	23.6395(10)	43.475(2)	24.9620(6)	30.2981(6)
α, deg	66.488(2)	105.992(2)	90	90	90
β, deg	69.768(2)	96.730(2)	90	91.5564(11)	113.8988(10)
γ, deg	85.210(2)	93.088(2)	90	90	90
V, (Å^3)	1255.40(8)	6390.9(5)	12785.2(10)	5962.9(3)	15508.0(6)
ρ_{calc}, g/cm^3	1.163	1.361	1.338	1.391	1.313
θ_{max}, deg	27.35	23.00	22.50	27.52	22.98
total data,[b] %	99.9	99.8	99.9	99.7	100.0
μ, mm^{-1}	0.786	1.064	1.063	1.137	0.984
R_1 (wR_2),[c] %	4.14 (10.33)	5.91 (9.27)	4.14 (8.72)	4.64 (9.46)	6.86 (14.66)
S[d]	1.026	1.022	1.020	1.021	1.033

[a] Data collected at T = 170(2) (for **3**) or 200(2) (all others) K using Φ and ω scans with graphite-monochromatized Mo Kα radiation (λ = 0.71073 Å). [b] Percent completeness of (unique) data collection within the θ_{max} limit. [c] Calculated for $I > 2\sigma(I)$: $R_1 = \sum||F_o| - |F_c||/\sum|F_o|$, $wR_2 = \{\sum w(F_o^2 - F_c^2)^2/\sum w(F_o^2)^2\}^{1/2}$. [d] S = goodness of fit = $\{\sum[w(F_o^2 - F_c^2)^2]/(n-p)\}^{1/2}$, where n is the number of reflections and p is the number of parameters refined.

(**b**) **Control Assays.** The efficiency and recovery limits of the benzoylation procedure were tested using $^{i}PrNH_2$, $^{i}PrNHNHP^{i}r$, and $HN(SiMe_3)_2$. A known amount of neat amine or hydrazine (typically 10 μL) was dissolved in aqueous 6 M HCl with stirring. The solution was chilled in an ice bath and made basic to litmus by addition of 5 M NaOH. The solution was treated with $NaHCO_3$ (0.25 g), followed by benzoyl chloride (1.1 equiv per nitrogen atom), then stirred vigorously for 1−2 h. The resulting mixture was extracted into CH_2Cl_2, dried over anhydrous Na_2SO_4, and filtered. After addition of a known quantity of internal integration standard (benzophenone), the solution was analyzed by GC to determine the recovery of amine or hydrazine as benzoylated species. The effect of iron on this protocol was assessed by the introduction of $FeCl_2$ or $FeCl_3$ (typically 20 mg) prior to the addition of amine or hydrazine. The presence of the iron chlorides resulted in the formation of gelatinous solids after basification with NaOH (green-colored from $FeCl_2$, perhaps $Fe(OH)_2$, and rust-colored from $FeCl_3$, perhaps FeO(OH)); $FeCl_2$, in particular, hindered the quantitation of organonitrogen products by GC. The addition of Na_2EDTA chelating agent prior to basification was successful in solubilizing the metal ions and improving the recoveries of benzoylated products. Limited hydrazine reduction (ca. 5%) was observed in the presence of iron salts.

The recovery of azobenzene was determined by the following procedure. Azobenzene (typically 20 mg) was dissolved in 2 mL of C_6H_6 and agitated with 3 mL of 6 M HCl for 1−2 h. The mixture was then extracted into CH_2Cl_2, partitioned, and dried over anhydrous Na_2SO_4. After filtration, a known amount of internal integration standard (anthracene) was added and the solution analyzed by GC. The addition of either $FeCl_2$ or $FeCl_3$ (10 mg) to the 6 M HCl solution before the addition of the azobenzene solution was found to have no effect on the GC analysis. Important control analyses are summarized in Table 6.

(**c**) **Reference Compounds.** Benzoylated reference compounds **^{i}PrNHBz**, **PhNHBz**, ***p*-TolNHBz**, **^{i}Pr(Bz)N−NHBz**, **^{i}Pr(Bz)N−NH^{i}Pr**, **^{i}Pr(Bz)N−N(Bz)^{i}Pr** were prepared by modification of the derivatization protocol described in parts (a) and (b). Compound identities were verified by GC/MS, ^{1}H NMR spectroscopy, and melting point comparison with literature values. Synthesis and characterization details are provided as Supporting Information.

X-ray Crystallography. Single crystals suitable for X-ray diffraction analysis were obtained from the following conditions: **2** as yellow-orange blocks, from THF/*n*-pentane solution at −30 °C; **3a** and **3b** as black plates, from C_6H_6/*n*-pentane vapor diffusion at 25 °C; **4** as black plates, from THF/*n*-pentane vapor diffusion at 25 °C.

General crystallographic procedures are detailed elsewhere.[51] ψ-Scan absorption corrections were applied using the Siemens SHELXTL software suite,[52] and multiscan absorption corrections were applied using PLATON.[53] Appropriate disorder models and restraints were employed as needed. Essential crystallographic data for the compounds in this work are summarized in Table 7, with specific details for individual structure determinations available as Supporting Information.

Acknowledgment. This research was supported by the Arnold and Mabel Beckman Foundation (Beckman Young Investigator Award), the National Science Foundation (U.S.A., CAREER CHE-9984645), and the Natural Sciences and Engineering Research Council (Canada). We thank Prof. R. Cava and Dr. T. Klimczuk (Princeton) for magnetochemical measurements, Prof. R. H. Holm (Harvard) for access to a Mössbauer spectrometer, and Lay Ling Tan for experimental assistance.

Supporting Information Available: Crystallographic data; syntheses and characterization data for reference compounds. This material is available free of charge via the Internet at http://pubs.acs.org.

(51) Kayal, A.; Ducruet, A. F.; Lee, S. C. *Inorg. Chem.* **2000**, *39*, 3696.
(52) Sheldrick, G. M. *SHELXTL*, Version 5.04; Siemens Analytical X-ray Instruments: Madison, WI, 1996.
(53) Spek, A. L. *Acta Crystallogr., Sect. A: Found. Crystallogr.* **1990**, *46*, C34.